

Einstein-Podolsky-Rosen entanglement in two-well BEC systems: ground states

Q. Y. He, P. D. Drummond,* and M. D. Reid†

*Centre for Atom Optics and Ultrafast Spectroscopy,
Swinburne University of Technology, Melbourne 3122, Australia*

We consider how to generate and detect Einstein-Podolsky-Rosen (EPR) entanglement and the EPR-steering paradox between groups of atoms in two separated potential wells in a Bose-Einstein condensate (BEC). We present experimental criteria for this form of entanglement, and propose experimental strategies using adiabatic cooling to the ground state. These approaches use either two or four spatial and/or internal modes. We also present higher order criteria that act as signatures to detect the multiparticle entanglement present in this system. We point out the difference between spatial entanglement using separated detectors, and other types of entanglement that do not require spatial separation. The four-mode approach with two spatial and two internal modes results in an entanglement signature with spatially separated detectors, conceptually similar to the original EPR paradox.

I. INTRODUCTION

The Einstein-Podolsky-Rosen (EPR) paradox [1] established a link between entanglement and nonlocality [2] in quantum mechanics. The extent to which entanglement can exist in spatially separated macroscopic and massive systems is still essentially unknown. Entanglement in optics however has been extensively studied and numerous experiments have shown evidence for it [3–7]. An important distinction is that optical entanglement involves (nearly) massless particles, and hence is a much less rigorous test of any gravitational effects present.

Generation of EPR entanglement between two massive systems therefore represents an important challenge. Such entanglement is a step in the direction of fundamental tests of quantum mechanics, and is relevant to the long term quest for understanding the relationship between quantum theory and gravity. Ultimately, one would like to demonstrate spatially entangled mass distributions, and this appears much more promising for ultra-cold atoms than for room-temperature atoms. For this reason, we focus on ultra-cold BEC environments here. This is also relevant if BEC interferometry is to be useful to those areas of quantum information and metrology where entanglement is known to give an advantage [8–13]. In this paper, we study strategies for generation of EPR entanglement between Bose-Einstein condensates (BEC) confined to two spatially separated potential wells.

Quantum correlations and EPR tests for Bose-Einstein condensates have been suggested previously, with strategies involving molecular down-conversion [14] and four wave mixing interactions [15–17], among others. Early experiments measuring free-space correlations demonstrated promising signatures of increased fluctuations associated with entanglement [18, 19], but were unable to conclusively demonstrate entanglement or squeezing via reduced fluctuations, largely due to measurement inefficiencies.

This has improved with recent multi-channel plate detection methods, but detection efficiency still remains an issue [20]. Entanglement has also been measured, very recently, for distinct but nearly spatially superimposed modes [21–23] in an optical lattice.

Here, we are motivated to study the two well case, in view of experiments that have used this or similar systems to confirm both sub-shot noise quantum correlations [24], and multiparticle entanglement among a small group of atoms [25, 26]. For much larger numbers of atoms ($\sim 40,000$), nearly quantum limited interferometry has been recently verified [27], showing that trapped atom interferometry has the potential to reach mesoscopic sizes. There have also been a number of previous theoretical studies [28, 29] that outline different proposals and entanglement signatures.

The goal of this paper is to clarify what it means to have an EPR entanglement between groups of atoms in a BEC, and outline some different strategies for achieving this goal. We define EPR entanglement as being that entanglement existing, at least in principle, between two spatially separated systems, so that it could potentially realize an EPR paradox. For EPR entanglement to be claimed, three properties must be evident [30]:

1. Two systems must be shown entangled through local measurements at spatially distinct locations.
2. The nature of the entanglement criterion should be to confirm an EPR paradox. This requires measurement of sufficiently strong correlation between the two systems, for two non-commuting “EPR” observables like position and momentum [7]. A more sophisticated approach would allow other entanglement measures, such as those for “EPR steering” [31–36] which reveal an inconsistency between EPR’s local realism and the completeness of quantum mechanics for other types of measurement strategies.
3. To justify EPR’s no “spooky action-at-a-distance” assumption [1], the measurement events should be causally separated.

* pdrummond@swin.edu.au

† mdreid@swin.edu.au

For large groups of atoms, the task of detecting EPR entanglement is much more feasible when the emphasis is on the EPR paradox itself, rather than on the failure of Bell's local hidden variable model [2]. For spatially separated systems, the detection of sufficient correlation of locally defined EPR observables so that entanglement is confirmed [37–39] would represent an achievable first benchmark. This by itself is not direct evidence for the EPR paradox, although it is a necessary condition. The second step of confirming the paradox has been carried out for photons [30], and also appears achievable for atoms. The last step is probably the most difficult for atoms. It would require either very fast measurements in one vacuum chamber, or hybrid techniques involving two separated BECs with coupling via atom-photon interfaces [40], in order to achieve causally separated measurement.

There are many possible strategies for generation of spatial EPR entanglement. Early experiments employed two photon cascades and, later, optical parametric down conversion, to generate entangled photon pairs [3–5]. Continuous variable EPR entanglement between two fields, in a so-called “two-mode squeezed state” [41], was also generated using parametric down conversion [6, 7, 42]. Such entanglement gave evidence for an EPR paradox [30], although true causal separation of measurement events was not demonstrated in these experiments.

The paper is arranged as follows. In Section II we give a general introduction to the different possible entanglement strategies. Section III focuses on signatures for demonstrating entanglement, as well as the hierarchy of nonlocality measures including EPR-steering and Bell indicators. Section IV considers entanglement preparation in a two-well system, modeled as two modes with boson operators a and b . In this case, the S-wave scattering *intra-well* interactions, given by Hamiltonians $H = ga^\dagger a^2$ and $H = gb^\dagger b^2$, provide the local nonlinearity at each well, while the coupling or tunneling *inter-well* term, modeled as $H = \kappa(a^\dagger b + ab^\dagger)$ generates inter-well entanglement. Here the intra- and inter-well interactions act *simultaneously*, in the adiabatic formation of the ground state. Section V treats a four-mode generalization of this. This has the advantage that EPR-entanglement can be measured using atom counting at each site, without the use of a local oscillator. Our conclusions are summarized in Section VI, with technical details given in the Appendices. This paper is based on the preliminary ideas presented in a Letter [29]. A second class of entanglement strategies using dynamical techniques will be analyzed in a subsequent paper.

II. ENTANGLEMENT STRATEGIES

A. Prototype states for two-mode entanglement

Suppose two spatially separated systems are describable as distinct modes, represented by boson operators

a and b . There are two prototype states that one can consider, that can give multiparticle EPR entanglement. The first, which we call particle-pair generation, is currently the most widely known and used [7]. We consider an entangled state with number correlations:

$$|\psi\rangle_{II} = \sum_{n=0}^{\infty} c_n |n\rangle_a |n\rangle_b. \quad (\text{II.1})$$

This type of two-mode squeezed state gives two-particle correlations arising from a pair production process $H = \kappa a^\dagger b^\dagger + \kappa^* ab$ where $\langle ab^\dagger \rangle = 0$ but $\langle ab \rangle \neq 0$, and the number difference is always squeezed [43, 44]. These EPR states are formed in optics with parametric down conversion [30], and similarly in nondegenerate four wave mixing [45]. Since they are **not** number-conserving, they are not typical of states formed in coupled two-well experiments, although they have been generated in recent BEC experiments using spin or mode-changing collisions [21–23]. We note that a full analysis of such a system requires consideration of the dynamics of the coupling to the pump that supplies the pairs of atoms. Generally, there is a back-reaction on the pump mode, causing excess phase-noise that limits amount of squeezing or entanglement that can be generated [46, 47].

In this paper, we will focus on a second form of EPR entanglement, which we call number conserving. This occurs, for example, when fixed number states are input into a beam splitter: $H = \kappa(a^\dagger b + ab^\dagger)$, so that $\langle ab \rangle = 0$ but $\langle ab^\dagger \rangle \neq 0$. We consider an entangled number-conserving state of form [48–53]:

$$|\psi\rangle_I = \sum_{n=0}^N c_n |n\rangle_a |N - n\rangle_b. \quad (\text{II.2})$$

This is similar to the states generated in optical fiber pulsed squeezing [54], and is the closest to the state prepared in some recent two-well BEC experiments, where the total number is conserved [24, 25]. We will examine situations with number anti-correlated states prepared through evaporative cooling and adiabatic manipulations near the ground state of a coupled-well system, as shown in Fig. 1.

B. Experimental strategies

Before examining detailed solutions for an interacting BEC, it is useful to summarize how two-mode number-conserving entanglement can be generated, in schematic form. We consider how to generate entanglement between two groups of atoms in separated potential wells in a BEC. What is useful is a combination of *nonlinear local* interactions to generate a nonclassical squeezed state in each well - together with a *nonlocal linear* interaction to produce the entanglement between two spatially distinct locations. In the case of the BEC, the S-wave scattering can provide a nonlinear local interaction, and

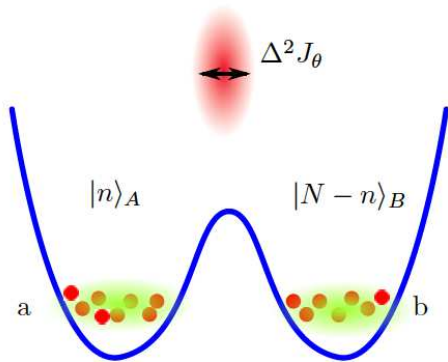


Figure 1. (Color online) A double-well, one spin orientation BEC. \hat{a}, \hat{b} are operators for two modes at A and B . The \hat{a} and \hat{b} are prepared with a two mode number difference squeezing and an entanglement, by adiabatic cooling to the ground state. In Section V, we develop signatures to detect the inter-well entanglement, using inter-well spin operators.

quantum diffusion across a potential barrier acts like a beam-splitter to provide the final nonlocal linear interaction. Both effects occur at the same time in the schemes treated here, in Sections IV and V.

We will show in Section IV that the entanglement generated for the two-well ground state with a fixed number of atoms can translate to an EPR steering type of entanglement [32, 36] (Fig. 1). For an *actual* demonstration of this sort of EPR entanglement, however, one must use signatures that involve local measurements, for two spatially separated observers (often called Alice and Bob), at sites A and B . One can use local oscillator (LO) measurements at each site, that provide phase shifts or their equivalent between the measured and LO modes [16]. Here, we propose an alternative though similar four-mode strategy, as shown in Fig. 2. We consider two types of *gedanken-experiment* as follows:

- **Two-mode entanglement preparation then analysis:** suppose the initial state is entangled through state preparation in a double-well potential. Here the nonlinearity occurs during state preparation, and the other steps are to enable the entanglement to be transformed into an easily measurable form. Experimentally, this appears relatively simple, although obtaining measurable signatures can be a challenge if strictly local measurements are used, as in an EPR paradox demonstration. This strategy is discussed in Section IV.
- **Four-mode entanglement preparation then analysis:** we consider four-mode states created through evaporative cooling and adiabatic processing in a double-well potential with two spin states in each well. Experimentally, this is more complex, but obtaining measurable signatures only requires local measurements in each well. This strategy is discussed in Section V.

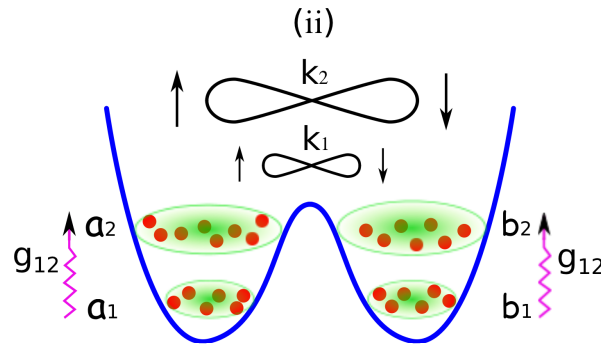


Figure 2. (Color online) A double-well, two spin orientation BEC. We suppose the modes a_i and b_i are spatially separated. Modes a_1, a_2 could be different spatial modes, or different spin components of the same well. Pairs a_1, b_1 (and a_2, b_2) can become entangled, due to the inter-well couplings. We allow for the asymmetric case where pair a_2 and b_2 have much greater numbers than a_1 and b_1 ($N_2 \gg N_1$) and also consider a case where modes a_2 and b_2 need not be entangled ($\kappa_2 = 0$).

In both two and four mode cases, the basic idea is:

1. Correlated ground state preparation, through evaporative cooling in a potential well *with linear coupling between wells*.
2. Local Rabi rotation to a superposition of internal spins, thus choosing an EPR measurement angle.
3. Measurement, usually from absorption imaging, giving occupation numbers.

III. MEASUREMENT STRATEGIES

A. Particle-pair EPR entanglement

In the EPR proposal [1], the paradox arose from correlations between the positions and momenta of two particles emitted from the same source. With optical or atomic Bose fields, one can define the quadrature phase amplitudes of the modes, as $X_A = a^\dagger + a$, and $Y_A = (a^\dagger - a)/i$, and similarly for mode b . These have the same commutators as position and momentum in a particle system. These quadratures, which are measured using local oscillators, can be used to detect the entanglement of the pair-correlated states discussed above, as performed recently for atoms by Gross et al [22].

1. Entanglement

The original EPR paradox focused on states that showed correlation and anti-correlation for position and momentum respectively. Duan et al and Simon [37, 38] showed that entanglement between modes a and b is confirmed if

$$\Delta^2(X_A - X_B) + \Delta^2(P_A + P_B) < 4. \quad (\text{III.1})$$

In the case (III.1), the 4 arises from the commutation relation $[a, a^\dagger] = 1$, and reflects the quantum noise associated with the four observables.

A full analysis of a local oscillator measurement shows that it is actually equivalent to a spin measurement, and closely related entanglement measures have been developed for use with spin measurements. In particular, one can show entanglement using the spin version of (III.1) [55],

$$\Delta^2(J_A^X \mp J_B^X) + \Delta^2(J_A^Y \pm J_B^Y) < |\langle J_A^Z \rangle| + |\langle J_B^Z \rangle|, \quad (\text{III.2})$$

and also the (more sensitive) Heisenberg-product entanglement criterion [39]

$$\sqrt{\Delta^2(J_A^\theta - J_B^\theta) \cdot \Delta^2(J_A^{\theta+\pi/2} + J_B^{\theta+\pi/2})} < \frac{|\langle J_A^Y \rangle| + |\langle J_B^Y \rangle|}{2}. \quad (\text{III.3})$$

2. EPR paradox entanglement

EPR's argument assumes that one observer (Alice) can make precise predictions for the outcome of position or momentum measurements made by a second, distant observer (Bob). To quantitatively demonstrate the EPR paradox, the level of correlation in Alice's predictions is compared with the quantum limit for a local state that might predetermine Bob's statistics. Thus, for the EPR paradox, the relevant quantum noise level is that of *one* observer, B , alone, which implies a stricter condition formulated in terms of conditional variances [7]. EPR paradox entanglement is observed when

$$\Delta(X_B|X_A)\Delta(P_B|P_A) < 1. \quad (\text{III.4})$$

Since the precise choice of measurement at mode A is not important, only the inference, this criterion is sometimes more generally written as $\Delta_{inf} X_B \Delta_{inf} P_B < 1$. In the case of (III.1), the stricter condition

$$\Delta^2(X_A - X_B) + \Delta^2(P_A + P_B) < 2 \quad (\text{III.5})$$

if satisfied would imply an EPR paradox entanglement [16, 30].

While the signatures (III.1-III.5) have been used extensively in relation to EPR-type entanglement, we do not use them in this paper. Evaluating, we find in fact

$$\begin{aligned} D &= \Delta^2(X_A - X_B) + \Delta^2(P_A + P_B) \\ &= 4(1 + \langle a^\dagger, a \rangle + \langle b^\dagger, b \rangle - \langle a, b \rangle - \langle a^\dagger, b^\dagger \rangle) \end{aligned}$$

(where here we use the conventional notation that $\langle x, y \rangle = \langle xy \rangle - \langle x \rangle \langle y \rangle$). Since detection of EPR entanglement using this criterion requires at least $D < 4$, we see that if $\langle a \rangle = \langle b \rangle = 0$, then $\langle ab \rangle \neq 0$ is a minimal requirement to use this signature. Where the number N of atoms is *fixed*, the ground state solution is of the form (II.2), for which $\langle ab \rangle = 0$. For this reason, we focus on a different set of EPR entanglement criteria.

B. Hillery and Zubairy type entanglement

The signatures given above are not the only possible ones, and in fact there are many signatures both for entanglement and the EPR paradox. A particularly useful alternative form was proposed by Hillery and Zubairy [56], and Cavalcanti et al [36, 57], as described and generalized below.

1. HZ entanglement criterion

Modes a and b are entangled if [56]

$$|\langle a^m (b^\dagger)^n \rangle|^2 > \langle (a^\dagger)^m a^m (b^\dagger)^n b^n \rangle. \quad (\text{III.6})$$

This criterion is useful for states with a large phase moment $\langle ab^\dagger \rangle$, as will be studied in Section V. In Ref [29] it was suggested how to rewrite this criterion for $m = n$. For any nonhermitian operator Z , we consider the generalized variance, which must be nonnegative:

$$\Delta^2 Z \equiv \langle (Z^\dagger - \langle Z^\dagger \rangle)(Z - \langle Z \rangle) \rangle = \langle Z^\dagger Z \rangle - \langle Z^\dagger \rangle \langle Z \rangle \geq 0. \quad (\text{III.7})$$

Defining $Z = a^m (b^\dagger)^m$, we find it is always true (for any state) that

$$|\langle a^m b^{\dagger m} \rangle|^2 - \langle a^{\dagger m} a^m b^{\dagger m} b^m \rangle \leq \langle a^{\dagger m} a^m (|b^m b^{\dagger m}, b^{\dagger m} b^m|) \rangle. \quad (\text{III.8})$$

Thus, the HZ criterion (III.6) confirms entanglement if:

$$0 \leq E_{HZ}^{(m)} = 1 + \frac{\langle a^{\dagger m} a^m b^{\dagger m} b^m \rangle - |\langle a^m b^{\dagger m} \rangle|^2}{\langle a^{\dagger m} a^m (b^m b^{\dagger m} - b^{\dagger m} b^m) \rangle} < 1. \quad (\text{III.9})$$

It is also possible to derive a criterion using the commutators for mode a . Hence the HZ entanglement criterion (III.9) is best written with the optimal choice of denominator, corresponding to the minimum of $\langle a^{\dagger m} a^m (b^m b^{\dagger m} - b^{\dagger m} b^m) \rangle$ or $\langle b^{\dagger m} b^m (a^m a^{\dagger m} - a^{\dagger m} a^m) \rangle$.

The *first order* ($m = n = 1$) HZ criterion for entanglement becomes

$$0 < E_{HZ}^{(1)} = 1 + \frac{\langle a^\dagger a b^\dagger b \rangle - |\langle ab^\dagger \rangle|^2}{\min\{\langle a^\dagger a \rangle, \langle b^\dagger b \rangle\}} < 1. \quad (\text{III.10})$$

The *second order* HZ entanglement criterion is obtained by using the power $m = 2$ with the identity $[b^2 b^{\dagger 2}, b^{\dagger 2} b^2] = 4b^\dagger b + 2$. Entanglement is then observed if

$$0 \leq E_{HZ}^{(2)} = 1 + \frac{\langle a^{\dagger 2} a^2 b^{\dagger 2} b^2 \rangle - |\langle a^2 b^{\dagger 2} \rangle|^2}{\langle a^{\dagger 2} a^2 (4b^\dagger b + 2) \rangle} < 1. \quad (\text{III.11})$$

We show in Appendix B that the higher order criteria with $m > 1$ are useful for detecting a multi-particle entanglement.

2. HZ EPR-steering

Criteria similar to III.6 that reveal not just entanglement, but the EPR-steering paradox [1, 7, 32, 35] or violation of local hidden variable theories (Bell's theorem) [2], have been derived in Refs [36] and [57]. In this paper, we consider two sites only, and focus on the entanglement and EPR-steering cases, since the Bell inequality derived in Ref [57] requires at least three sites.

The terminology “EPR-steering” is used to describe a more general EPR paradox situation that can involve any type of measurement, not just conjugate spins or position/momentum [32, 35]. The EPR paradox was discussed by Schrodinger [31], who pointed to the phenomenon of “steering”. Criteria for “steering” can be developed using the asymmetric local hidden state separable model developed in Ref. [32]. Analysis tells us that violation of this model reveals inconsistency of local realism with the completeness of quantum mechanics, and is thus also a criterion for a generalized EPR paradox [30, 32, 33, 35].

An EPR-steering nonlocality is detected if

$$|\langle a^m b^{\dagger n} \rangle|^2 > \langle a^{\dagger m} a^m (\frac{b^{\dagger n} b^n + b^n b^{\dagger n}}{2}) \rangle. \quad (\text{III.12})$$

The proof follows from straightforward application of methods is given in [36] which derived the EPR steering result for $m = n = 1$. Similar higher moment extensions of the CFRD Bell nonlocality [57] have been considered in [58]. This criterion can also be rewritten in terms of the HZ entanglement parameter (III.10), so that *EPR-steering entanglement* is confirmed if:

$$0 \leq E_{HZ}^{(m)} = 1 + \frac{\langle a^{\dagger m} a^m b^{\dagger m} b^m \rangle - |\langle a^m b^{\dagger m} \rangle|^2}{\langle a^{\dagger m} a^m (b^m b^{\dagger m} - b^{\dagger m} b^m) \rangle} < \frac{1}{2}. \quad (\text{III.13})$$

IV. GENERATION OF NUMBER-CONSERVING TWO-MODE ENTANGLEMENT

We next turn to physical means to generate and measure entanglement and EPR-steering in two-mode physical systems. We focus here on the *gedanken*-experiment of Fig 1, with explicit spatial separation of the two modes. Of course, one can use these criteria to discuss entanglement of two spin degrees of freedom as well, but unless these are localized with a spatial separation, there is no causal separation possible: and hence no EPR interpretation.

A. Spin-operator HZ criterion

It is convenient to quantify entanglement in the number-conserving case using spin-operator methods.

Hillery and Zubairy [56] have written the first order criterion (III.10) in terms of the variances of inter-well Schwinger spins, defined as:

$$\begin{aligned} J_{AB}^X &= (a^\dagger b + ab^\dagger) / 2 \\ J_{AB}^Y &= (a^\dagger b - ab^\dagger) / (2i) \\ J_{AB}^Z &= (a^\dagger a - b^\dagger b) / 2 \\ J_{AB}^2 &= \hat{N}(\hat{N} + 2) / 4 \\ \hat{N}_{AB} &= a^\dagger a + b^\dagger b. \end{aligned} \quad (\text{IV.1})$$

Where the outcomes for \hat{N}_{AB} are fixed, the spin is fixed as $J = N/2$. The resulting ground-state HZ entanglement criterion is given by Eq. (III.10) which can also be written as:

$$0 < E_{HZ} = \frac{(\Delta J_{AB}^X)^2 + (\Delta J_{AB}^Y)^2}{\langle \hat{N}_{AB} \rangle / 2} < 1. \quad (\text{IV.2})$$

It should be noted here that this type of spin-operator variance has been measured experimentally [24] by observing the interference between the two modes, on expanding the atomic clouds after turning the traps off. However, as we discuss later, this strategy cannot be readily interpreted in the EPR sense, due to the lack of separation during measurement.

The best entanglement as measured by (IV.2) is given when the sum of the two variances of J_{AB}^X and J_{AB}^Y is minimized. This sum can *never* be zero, meaning that ideal entanglement of $E_{HZ} = 0$ cannot be reached, because the spins J_{AB}^X and J_{AB}^Y do not commute. However, the sum becomes asymptotically small for large N , in which case large noise appears in the third spin J_{AB}^Z . The lower bound for the sum of the two variances has been obtained by [59]:

$$\frac{(\Delta J_{AB}^X)^2 + (\Delta J_{AB}^Y)^2}{J} \geq C_J / J \quad (\text{IV.3})$$

where the coefficients C_J are given in that reference. The reduction of the sum $(\Delta J_{AB}^X)^2 + (\Delta J_{AB}^Y)^2$ below the standard quantum limit (given by $J = \langle \hat{N}_{AB} \rangle / 2$) is referred to as “planar squeezing”, and represents the onset of HZ entanglement.

The inequality (IV.3) leads to a useful result that will be used later in Section IV. Since a large spin J can only be obtained where the number of atoms N is large, very small squeezing necessarily implies an entangled state with a large mean $\langle N \rangle$. A full analysis is given in the Appendix A. This type of approach has been used by Sorenson and Molmer [60], where measurements are made of the variance of J_Z , and has proved useful in deducing multiparticle entanglement [25, 26].

B. Beam splitter with fixed number input states

Possibly the simplest number-conserving entangled state is obtained with a number-squeezed input, together

with a beam splitter interaction

$$H = \kappa a^\dagger b + \kappa^* a b^\dagger, \quad (\text{IV.4})$$

which models the exchange of atoms that can take place between wells.

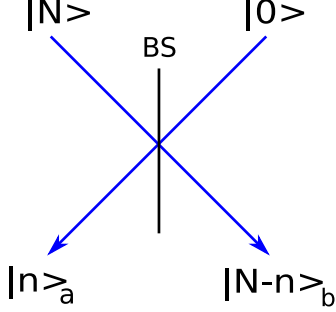


Figure 3. (Color online) A Fock number state $|N\rangle$ incident on a beam splitter produces an entangled state (II.2).

On defining output (a, b) , input (a_{in}) and vacuum (a_v) input modes (Fig. 3, 5), one can write the beam splitter transformation as

$$\begin{aligned} a &= (a_{in} + a_v)/\sqrt{2} \\ b &= (a_{in} - a_v)/\sqrt{2}. \end{aligned} \quad (\text{IV.5})$$

1. Single number-state input

We first consider the simplest case of N atoms input to one port of the beam splitter (Fig. 3). This is equivalent to the linear interferometer case [25] in which a fixed number of atoms are initially in one BEC well. These are then redistributed between wells via a number conserving mechanism. Using IV.5, the final state is number-conserving (II.2):

$$|out\rangle = \sum_{n=0}^N c_n |n\rangle_a |N-n\rangle_b, \quad (\text{IV.6})$$

where $c_n = \sqrt{N!}/\sqrt{2^N n!(N-n)!}$. This state (IV.6) is entangled for all N . The entanglement can be detected using the Hillery and Zubairy entanglement measure (III.9). Higher order (up to N -th) entanglement is also evident using the $E_{HZ}^{(n)}$ criteria (Fig. 4).

This method generates a relatively small degree of entanglement, however, (Fig. 4), and will later be compared with the much more significant entanglement obtainable using nonlinear BEC interactions.

2. Double number state input

We next consider a double Fock number state $|N\rangle|N\rangle$ incident on a beam splitter (Fig. 5), as a model for

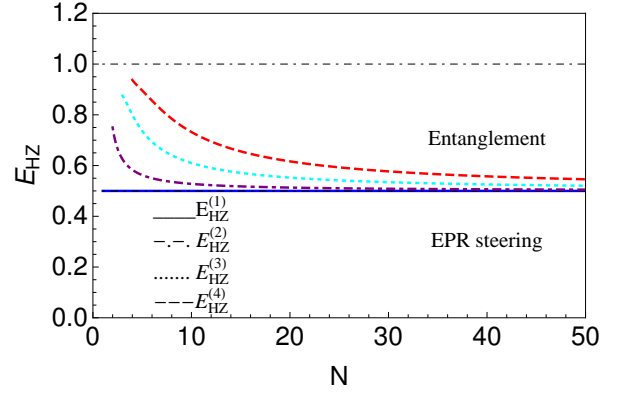


Figure 4. (Color online) A single Fock number state with beamsplitter is entangled ($E_{HZ} < 1$) by the HZ entanglement criteria, Eq. (III.9). Higher order entanglement is indicated by the dashed lines. The correlation does not confirm EPR-steering entanglement from Eq. (III.13), which requires $E_{HZ} < 0.5$.

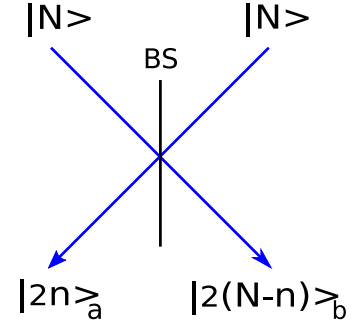


Figure 5. (Color online) A double Fock number state incident on a beam splitter also produces a number-conserving entangled state.

the case where there is initially a fixed, equal number of atoms in each well.

The output state after an exchange between the wells is

$$|out\rangle = \sum_{n=0}^N c_n |2n\rangle_a |2(N-n)\rangle_b \quad (\text{IV.7})$$

where $c_n = (-1)^{N-n} \sqrt{(2n)!} \sqrt{(2(N-n))!} / [2^N n!(N-n)!]$. In this case, entanglement is again present for all N , but cannot be detected via the first order entanglement criterion (III.10).

Entanglement can however be detected via the second order HZ entanglement criterion Eq. (III.11), which indicates an entanglement involving superposition are number states different by two particles. The fourth-order entanglement $E^{(4)}$ is also evident, indicating superpositions involving states separated by four particles. The entanglement measure $E^{(2)}$ is sufficiently strong that EPR steering can also be confirmed via Eq. (III.13) with $m = n = 2$, as shown in Fig. 6, though this is diminished at higher N .

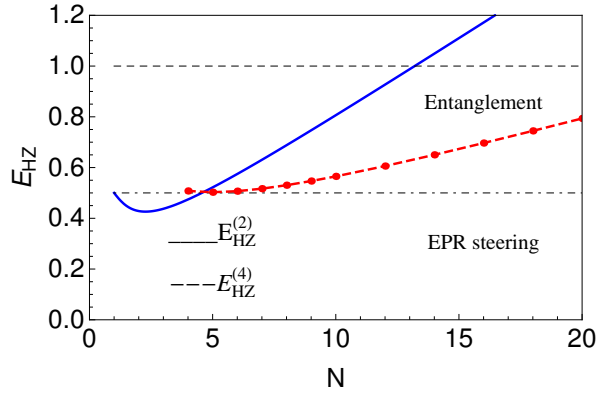


Figure 6. (Color online) HZ entanglement criterion using a double Fock number state and beam splitter. The graph shows the criterion (III.9) for $m = n = 2$ (solid blue line), and $m = n = 4$ (red dashed line). EPR-steering is observable with $m = n = 2$ and $N < 5$.

C. Nonlinear case: BEC ground state

We now examine how to enhance the entanglement over the linear case above, by using a local number-conserving nonlinearity.

1. Two-mode BEC Hamiltonian

We solve for the ground state of a two-component BEC (Fig. 1), as modeled by the following two-mode Hamiltonian:

$$H = \kappa(a^\dagger b + ab^\dagger) + \frac{g}{2}[a^\dagger a^\dagger aa + b^\dagger b^\dagger bb]. \quad (\text{IV.8})$$

Here κ denotes the conversion rate between the two components, denoted by the mode operators a and b , and $g \propto a_{3D}$ is the nonlinear self interaction coefficient[49], proportional to the three-dimensional S-wave scattering length, a_{3D} . The first term proportional to κ describes an exchange of particles between the two wells (modes) in which total number is conserved. This term is the linear term equivalent to that for a beam splitter. The second nonlinear term can be thought of as creating squeezing. It models nonlinearity in many systems, including dispersive optical bistability, from which squeezing is known to result. The Hamiltonian is a general one, and this model also applies to other systems such as optical cavity modes or superconducting wave-guides with a nonlinear medium.

The ground state obtained using standard matrix techniques, and only depends on the dimensionless ratio g/κ . We consider a total of N atoms: the number in well a is $\hat{N}_a = a^\dagger a$ and similarly, $\hat{N}_b = b^\dagger b$. Entanglement between the modes a and b , and hence between the two wells, can be detected via the first order HZ entanglement criterion Eq. (III.10), for both attractive ($g < 0$) and repulsive ($g > 0$) regimes, as shown in Figs. 7 and 8.

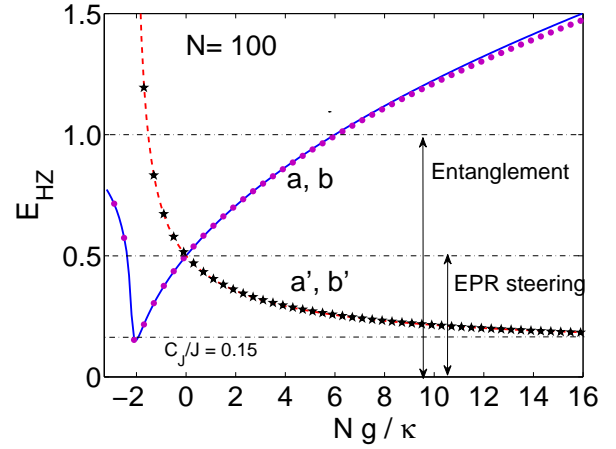


Figure 7. (Color online) Entanglement in the ground state of the BEC Hamiltonian Eq. (IV.8), using the HZ criterion Eq. (III.10), plotted against the coupling constant for both positive and negative couplings, for $N = 100$ atoms. Plots show HZ entanglement as a function of Ng/κ , with $\kappa > 0$ held fixed and g varied. The mean spin is in the direction defined by J_{AB}^X . $E_{HZ} < 1$ indicates a two-mode entanglement; $E_{HZ} < 0.5$ indicates EPR steering. The dashed red line gives the HZ criterion E'_{HZ} for the rotated modes a' and b' . The predictions for the respective second order entanglement criterion $E_{HZ}^{(2)}$ (Eq. (III.11)), are given by the dotted and starred curves.

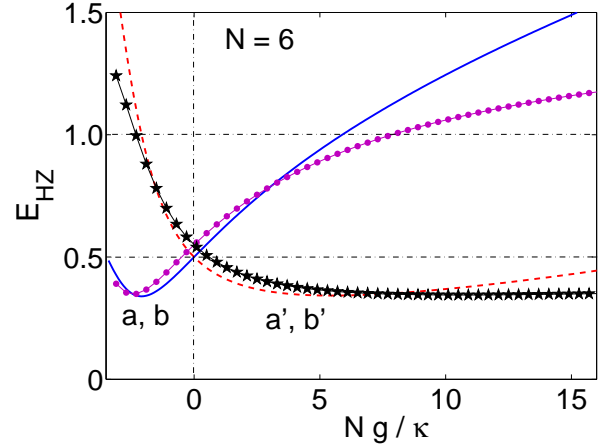


Figure 8. (Color online) Same as Fig. 7 but for much lower particle number, with $N = 6$. First order entanglement in (a, b) is shown by the solid blue line, with second order entanglement shown by the purple line with dots. First order entanglement in (a', b') is shown by the dashed red line, with second order entanglement shown by the black line with stars. The second order entanglement criterion becomes more sensitive where the nonlinearity is higher in both cases.

2. Attractive interactions

The best entanglement (i.e. the smallest possible value for E_{HZ}) is given when the sum of the two variances of J_{AB}^X and J_{AB}^Y is minimized. As explained above in Sec-

tion IV, this sum can never be zero, because the spins do not commute, meaning that ideal entanglement of $E_{HZ} = 0$ cannot be reached. The lower bound for the sum of the two variances has been obtained by [59] and is given by equation (IV.3). The reduction of the sum $(\Delta J_{AB}^X)^2 + (\Delta J_{AB}^Y)^2$ below the standard quantum limit (given by $J = \langle \hat{N}_{AB} \rangle / 2$) is referred to as “planar squeezing”, and represents the onset of HZ entanglement.

The absolute lower bound for E_{HZ} is predicted for the BEC ground state of (IV.8) in the attractive regime where g is negative, as shown for $N = 100$ in Fig. 7, and for $N = 6$ in Fig. 8. This critical case has been studied and explained in [59] and [61]. We note however that the minimum E_{HZ} becomes asymptotically small for large N , in which case large noise appears in the third spin J_{AB}^Z . The degree of entanglement increases with N the number of atoms, according to the relation for C_J obtained in [59].

For a given number of atoms N , the best possible HZ entanglement is thus

$$E_{HZ} = \frac{(\Delta J_{AB}^X)^2 + (\Delta J_{AB}^Y)^2}{\langle \hat{N}_{AB} \rangle / 2} \geq C_{N/2} / (N/2), \quad (\text{IV.9})$$

The experimental observation of $E_{HZ} < C_{n_0/2} / (n_0/2)$ implies that the two-mode entangled state consists of *more* than n_0 atoms in total, that is, that there are necessarily more than n_0 atoms entangled e.g. for $n_0 = 100$, this could be a state like $\{|50\rangle|51\rangle + |51\rangle|50\rangle\} / \sqrt{2}$. As explained in the Appendix A, the result follows because values of C_J/J for increasing J are a decreasing sequence, and thus a measured value of $C_J/J = 0.15$, for example, can only come from an entangled state with at least 100 atoms.

The best HZ inter-mode entanglement is achieved in the attractive regime. We note that the strongest theoretical entropic entanglement $\varepsilon(\rho)$ [62, 63] is found when all atom numbers are equally represented in the superposition. It is shown in [29] that the closest state to this optimum is obtained at a critical value of $Ng_{11}/\kappa \approx -2.0$, that is, the attractive interaction regime (as found in ^{41}K and ^7Li isotopes) gives rise to a maximal spread in the distribution of numbers in each well.

Interestingly, Fig. 7 shows the same point of maximum is observed for the higher order entanglement measure $E_{HZ}^{(2)}$. This measure can only detect entanglement that originates from superpositions of the type $|50\rangle|51\rangle + |51\rangle|50\rangle + |52\rangle|49\rangle$, where at least some of the states of the superposition are separated by 2 quanta (Appendix B). Similarly, the third order entanglement criterion $E_{HZ}^{(3)}$ detects entanglement originating from states separated by 3 quanta. In the case of Fig 7, where there is $N = 100$ quanta, the existence of entangled states such as $|0\rangle|100\rangle + \dots + |100\rangle|0\rangle$ could be detected by measuring $E_{HZ}^{(100)} < 1$. Higher order entanglement (e.g. $E_{HZ}^{(101)} < 1$) would not be possible.

3. Repulsive interactions

The repulsive regime of positive g also predicts considerable planar squeezing (Fig. 7), but, in that case, the best planar squeezing is rotated into the $X - Z$ plane as graphed in Fig. 9 [61, 64]. A depiction of the resulting planar squeezing ellipsoid is shown in Fig 10.

Thus, the corresponding HZ entanglement is between

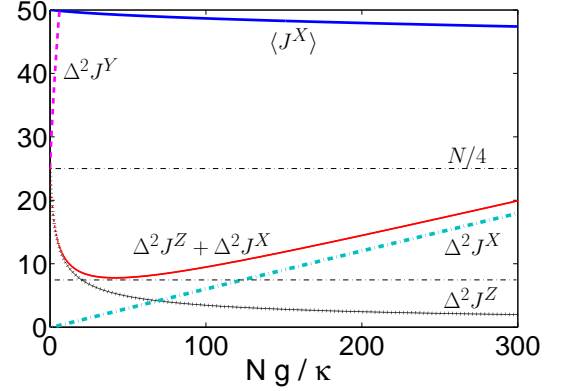


Figure 9. (Color online) The repulsive interaction case for $N = 100$, showing individual spin variances, and mean spin, $\langle J_{AB}^X \rangle$, for the ground state solution of Hamiltonian in the regime where there is a strong repulsive self-interaction g/κ , for $N = 100$. Here $\kappa > 0$ is fixed and g is varied.

the modes defined by the *rotated* coordinates,

$$a' = (a + b) / (\sqrt{2}i), \quad b' = (a - b) / \sqrt{2}. \quad (\text{IV.10})$$

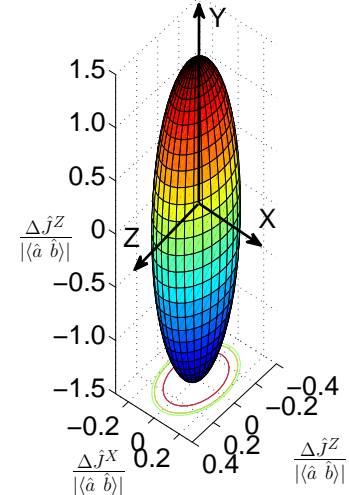


Figure 10. (Color online) The 3-D variance ellipsoid corresponding to $N = 100$ and a repulsive interaction at the optimum coupling of $Ng/\kappa = 40$. Spin variances are reduced in both axes parallel to the $X - Z$ plane, to show strong, but not perfect, planar quantum squeezing. The variance increases perpendicular to the squeezing plane, along the Y axis.

The corresponding entanglement criterion is given by:

$$0 < E'_{HZ} = \frac{(\Delta J_{AB}^X)^2 + (\Delta J_{AB}^Z)^2}{(\langle a^\dagger a \rangle + \langle b^\dagger b \rangle)/2}. \quad (\text{IV.11})$$

The detection of spatial HZ entanglement between the two wells in the repulsive case would therefore require a different detection scheme, as proposed in [61]. We note that in both repulsive and attractive cases, the HZ entanglement can be very significant, so that the EPR steering nonlocality Eq (III.13) is predicted via measurement of both the first and second order HZ moments. Figure 9 indicates that, for fixed N , the repulsive case shows an increasing and then reducing first order HZ entanglement (III.10), as the nonlinearity g/κ increases. The optimum case occurs for $N = 100$ and a repulsive interaction at a coupling of $Ng/\kappa = 40$. The squeezing ellipsoid for this coupling is shown in Fig 10.

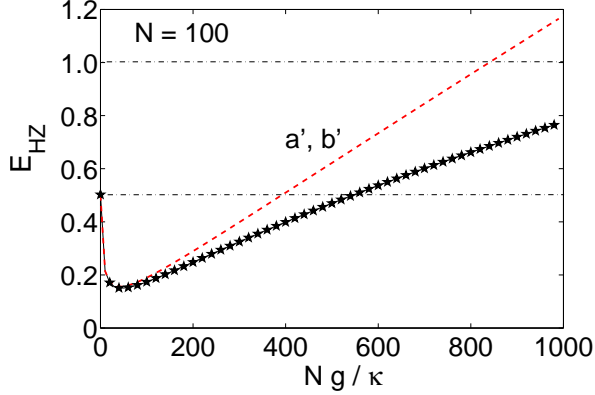


Figure 11. (Color online) Higher order entanglement for the case of $N = 100$. Other parameters as in 7. The red dashed line shows a reduced E_{HZ} entanglement as g/κ is increased above a certain level. The solid black line (starred) shows the second order entanglement. Here $E_{HZ}^{(2)} < 1$, indicating entanglement, is possible at higher g/κ ratios where the first order (dashed) criterion shows no entanglement.

Interestingly, however, from Fig. 11, we see that the second order entanglement criterion for $N = 100$ picks up more entanglement, suggestive that the drop is due to a change in the nature of the entanglement, rather than to a loss of entanglement itself. Fig. 8 shows that a similar behavior occurs at much lower particle number with $N = 6$, although with less overall entanglement at the optimum coupling.

The entanglement itself, via the measure of E_{HZ} , can be deduced via measurements of the combined spins J_{AB} , using interference measurements between the two condensates, as has been performed in [24]. Results obtained in this fashion are important in confirming the existence of that type of entanglement within quantum theory, but as the measurements are not localized at each site, they cannot be viewed as rigorous tests of EPR entanglement, EPR steering or nonlocality. In order to

use the above strategies to confirm an EPR-type entanglement, one would measure the local EPR observables, $X_{A/B}$ and $P_{A/B}$, at each well. This is because the moments of (III.6) are in terms of operators, a and b , which are linear combinations of the hermitian observables, X 's and P 's. Optically, the X and P are field amplitudes, the measurement of which is normally achieved by phase sensitive local oscillators [6].

V. EPR ENTANGLEMENT: FOUR COMPONENT CASE

We will show in this section how to use two additional modes per site to perform an effective “local oscillator” measurement in this BEC case. Similar strategies have been suggested by Ferris et al [16] among others.

A. Spin-operator entanglement criteria

A true EPR experiment would involve coherent combination of second fields or condensates at each site, as depicted schematically in Fig. 2. To observe true EPR entanglement between sites A, B , a useful procedure is to use two modes per EPR site. Local intra-well spin measurements are defined: for well A ,

$$\begin{aligned} J_A^X &= (a_1^\dagger a_2 + a_2^\dagger a_1) / 2, \\ J_A^Y &= (a_1^\dagger a_2 - a_2^\dagger a_1) / (2i), \\ J_A^Z &= (a_2^\dagger a_2 - a_1^\dagger a_1) / 2, \\ \hat{N}_A &= a_2^\dagger a_2 + a_1^\dagger a_1. \end{aligned} \quad (\text{V.1})$$

Here $a_{1,2}$ are mode operators for different components of the same site, typically different spatial modes or different nuclear spins at each site. We will also introduce the notation for the corresponding raising and lowering spin operators, $J_A^\pm = J_A^X \pm iJ_A^Y$. Similar spin operators are defined for site B . This defines complementary observables that are locally measurable at each site, using Rabi rotations and number-difference measurements. Calculations of spin correlations at two sites can be carried out most simply on imaging on a micron scale, then dividing the imaged atoms into two halves for measurement purposes. A more sophisticated method is to add a time-dependent external potential to divide the condensate into two widely separated parts. While this gives results that depend on the potential, it provides a physical separation between the sites.

Having defined local spin operators, we now need to consider a suitable EPR entanglement measure. We present HZ-type criteria that are expressed in terms of these effective local spin operators [65–67]. Entanglement is confirmed if

$$|\langle J_A^+ J_B^- \rangle|^2 > \langle J_A^+ J_A^- J_B^+ J_B^- \rangle. \quad (\text{V.2})$$

This inequality thus uses operators which are measurable locally using Rabi rotations and number measurements [25]. Criteria involving higher moments are also possible, but are not examined here. As for the original HZ criterion, the spin criterion can be rewritten using the procedure outlined in [29]. If we define $Z = J_A^+ J_B^-$, then we can easily show that $\Delta^2(J_A^+ J_B^-) = \langle J_A^+ J_A^- J_B^+ J_B^- \rangle - \langle [J_A^+, J_A^-] J_B^+ J_B^- \rangle - |\langle J_A^+ J_B^- \rangle|^2 \geq 0$. Thus,

$$|\langle J_A^+ J_B^- \rangle|^2 - \langle J_A^+ J_A^- J_B^+ J_B^- \rangle \leq \langle [J_A^-, J_A^+] J_B^+ J_B^- \rangle = 2\langle J_A^Z J_B^+ J_B^- \rangle. \quad (\text{V.3})$$

Similarly, defining $Z^\dagger = J_A^- J_B^+$, one can show that

$$|\langle J_A^+ J_B^- \rangle|^2 - \langle J_A^+ J_A^- J_B^+ J_B^- \rangle \leq 2\langle J_A^+ J_A^- J_B^Z \rangle. \quad (\text{V.4})$$

The spin entanglement criterion (V.2) becomes

$$E_{HZ}^{spin(1)} = \frac{\Delta^2(J_A^+ J_B^-)}{\min[2\langle J_A^Z J_B^+ J_B^- \rangle, 2\langle J_A^+ J_A^- J_B^Z \rangle]} < 1. \quad (\text{V.5})$$

i.e. HZ-type spin entanglement can then be verified if $0 \leq E_{HZ}^{spin(1)} < 1$.

Spin versions of the EPR paradox criteria (III.4-III.5) are possible [30, 68, 69], but here we focus on the spin EPR steering inequalities that relate to (V.2). These have been derived in [70]: EPR steering is detected if

$$|\langle J_A^+ J_B^- \rangle|^2 > \langle [(J_A)^2 - (J_A^Z)^2 \pm J_A^Z] \times [(J_B)^2 - (J_B^Z)^2] \rangle, \quad (\text{V.6})$$

which can be rewritten as

$$0 \leq E_{HZ}^{spin(1)} = 1 + \frac{\langle J_A^+ J_A^- J_B^+ J_B^- \rangle - |\langle J_A^+ J_B^- \rangle|^2}{\min[2\langle J_A^Z J_B^+ J_B^- \rangle, 2\langle J_A^+ J_A^- J_B^Z \rangle]} < \frac{1}{2}. \quad (\text{V.7})$$

We note the spin moments of Eqs (V.5) and (V.7) are *actually* measured via the x and y spin components, for example, using the expansion:

$$\langle J_A^+ J_B^- \rangle = \langle J_A^X J_B^X - i J_A^X J_B^Y + J_A^Y J_B^X + J_A^Y J_B^Y \rangle. \quad (\text{V.8})$$

B. Linear multimode case

We examine the linear case first, to model a fixed number of atoms with a minimal BEC nonlinear self interaction. Suppose a Fock number state $|\psi_{in}\rangle = |N_1\rangle_{a_{in1}} |N_2\rangle_{a_{in2}} |0\rangle_{b_{in1}} |0\rangle_{b_{in2}}$ is incident on a beam splitter (Fig. 12), so that N_1 and N_2 are fixed, and modes within each pair a_1, b_1 and a_2, b_2 are coupled by the BS interaction, with a_1 and a_2 (and b_1, b_2) remaining uncoupled. Output modes a_1 and b_1 are number-conserved according to (II.2); as is pair a_2, b_2 , and are given as $a_{1,2} = (a_{in1,2} + b_{in1,2})/\sqrt{2}$, and $b_{1,2} = (a_{in1,2} - b_{in1,2})/\sqrt{2}$. The output state is

$$|out\rangle = \sum_{n=0}^{N_1} \sum_{n'=0}^{N_2} c_{n,n'} |n\rangle_{a1} |n'\rangle_{a2} |N_1 - n\rangle_{b1} |N_2 - n'\rangle_{b2} \quad (\text{V.9})$$

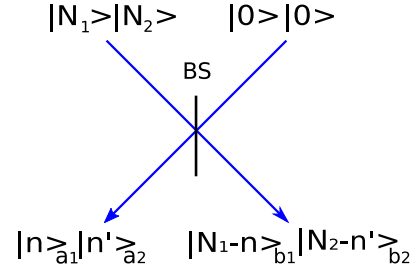


Figure 12. (Color online) We consider pairs of Fock states transmitted through a beam splitter. Pair a_1, b_1 are coupled and become entangled, as do a_2, b_2 .

where $c_{n,n'} = \sqrt{N_1!N_2!}/\sqrt{2^{N_1+N_2}n!(N_1-n)!n'!(N_2-n')!}$. We can evaluate moments, to obtain the prediction for the HZ spin criterion Eq. (V.5). Fig. 13 shows the result of varying N_1 for fixed $N_2 = 100$. The asymmetric case is favorable to detecting entanglement.

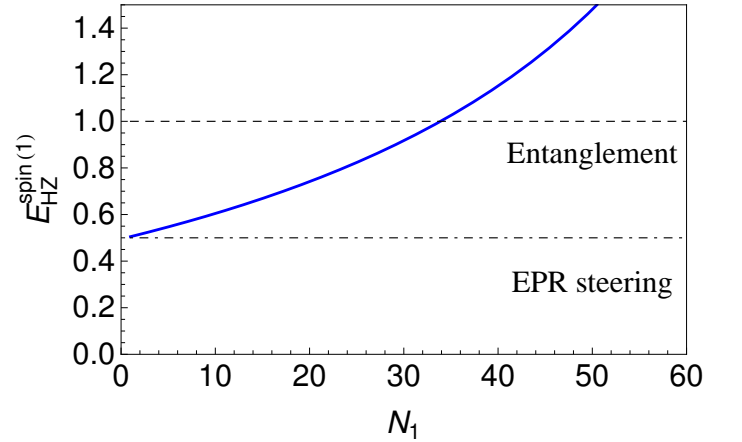


Figure 13. (Color online) The entanglement of pairs of Fock states transmitted through a beam splitter can be detected via criterion Eq. (V.5) for the asymmetric case where pair a_2 and b_2 have much greater numbers $N_2 \gg N_1$ ($N_2 = 100$). Entanglement is confirmed if $E_{HZ}^{spin(1)} < 1$.

Where the initial state is more complex, such as $|\psi_{in}\rangle = |N_1\rangle_{a_{in1}} |N_2\rangle_{a_{in2}} |N_1\rangle_{b_{in1}} |N_2\rangle_{b_{in2}}$, the output state will involve superpositions of only even numbers of atoms in the symmetric and antisymmetric modes, so that $|\langle J_A^+ J_B^- \rangle|^2 = |\langle a_2^\dagger a_1 b_2 b_1^\dagger \rangle|^2 = 0$. As in the case of Section IV.B.2, we can detect this entanglement using an appropriate second order spin criterion.

C. Nonlinear four component BEC case

We now consider the EPR entanglement that can be generated and measured when the modes interact to form the four-mode BEC ground state. We focus on set-ups that will enable the four mode case to produce an EPR entanglement that is the replica of the two-mode HZ en-

tanglement, as displayed in Figures (7-11). In this case, the second mode at each site may be thought of as part of a measurement system.

1. Four-mode BEC Hamiltonian

We assume the two-well, four-mode system of Fig 2 is described by the Hamiltonian:

$$\hat{H}/\hbar = \sum_i \kappa_i a_i^\dagger b_i + \frac{1}{2} \left[\sum_{ij} g_{ij} a_i^\dagger a_j^\dagger a_j a_i \right] + \{a_i \leftrightarrow b_i\}. \quad (\text{V.10})$$

We consider two modes at each EPR site A and B , with four modes in total, as shown schematically in Fig. 2. This corresponds to the two component per well experiments of [25], and somewhat less closely to the multi-mode interferometry experiments of [27]. Depending on the exact configuration, the local modes at each EPR site can be independent (in which case local cross couplings g_{ij} are zero ($g_{12} = 0$)), or not independent, as would be the case where the modes are coupled by the BEC self interaction term, so the couplings cannot be “turned off”, as in the set-up of [25]. The coupling constant is proportional to the three-dimensional S-wave scattering length, so that $g_{ij} \propto a_{ij}$, as in the two-mode case. For example, a typical value of the S-wave scattering length for ^{87}Rb is $a_{11} = 100.4a_0$, where a_0 is a Bohr radius. Zero cross couplings are likely require spatial separation of the two local modes, as might be achievable with four wells.

The Hamiltonian (V.10) with $\kappa = \kappa_1 = \kappa_2$ is based on the assumption that the second pair of modes a_2, b_2 are coupled between the wells in the same way as the first pair a_1, b_1 , which implies similar diffusion across wells. The case where $\kappa_2 = 0$, $\kappa_1 \neq 0$ is possible where diffusion across the wells can be controlled, as where the local modes represent separate wells. We will examine the predictions for both cases.

2. Symmetric tunneling case

The BEC nonlinearity can enhance the entanglement. This is evident on comparing with the case of zero atom-atom interaction ($g_{ij} = 0$), which corresponds to the result of the linear beamsplitter model (Fig. 12), and is indicated by the large red circles in the Figures 14-16. First, we examine the case of symmetric inter-well tunneling with $\kappa = \kappa_1 = \kappa_2$, so there is complete symmetry between the nonlocal setups, but a variable local cross coupling g_{12} . Figure 14 shows entanglement using the HZ spin criterion Eq. (V.5), for the ground state, for cases of both zero and strong local couplings g_{12} . Asymmetric atom numbers with $N_1 \ll N_2$ are required for the best entanglement, however, as shown in the inset of Fig. 14.

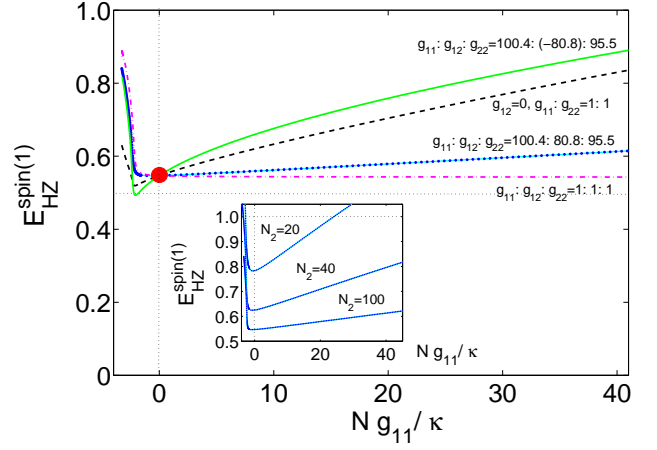


Figure 14. (Color online) Entanglement using adiabatic cooling to ground state in a two-well potential, at $T = 0K$, for the four mode model of Fig. 2, with a variety of local cross couplings g_{ij} . Here $\kappa = \kappa_1 = \kappa_2 > 0$ and g_{11} is varied with the other values of g_{ij} held in a fixed ratio, with $N_1 = 5$, $N_2 = 100$. $E_{HZ}^{spin(1)} < 1$ indicates entanglement; $E_{HZ}^{spin(1)} < 0.5$ indicates EPR steering. Curves are labelled in order of nesting as: (purple dash dotted) equal couplings; (blue dots) non-zero cross-couplings corresponding to ^{87}Rb Feshbach resonance with $a_{11} = 100.4a_0$, $a_{12} = 80.8a_0$, $a_{22} = 95.5a_0$; (black dashed) without cross-correlations $g_{12} = 0$; $g_{22} = g_{11}$; (green solid curve) negative relative cross-coupling $g_{11}g_{12} < 0$. The inset shows the effect of increasingly symmetric atom numbers.

We note from Fig. 14 that the entanglement is improved by using a “local oscillator”-type approach, in which the second modes a_2, b_2 are independent of the first at each location ($g_{12} = 0$) (being only combined at the spin measurement stage (V.1)) and are of much greater numbers ($N_2 \gg N_1$). In addition however, we note from the black dashed curve of Fig. 15 that better entanglement is obtained if the second “local oscillator” pair a_2, b_2 are *also* entangled optimally, as given by the critical point of the plots in Fig. 7. Thus, the optimal $E_{HZ}^{(1)}$ is at $N_2 g_{22}/\kappa_2 \approx -2.03$ for the modes a_2 and b_2 , and at $N_1 g_{11}/\kappa_1 \approx -2.1$ for modes a_1 and b_1 (as shown in the inset of Fig. 15). The choice $N_2 g_{22} \sim N_1 g_{11}$ therefore gives enhanced EPR spin entanglement (red solid curve of Fig. 14).

The minimum of $E_{HZ}^{spin(1)}$ corresponds to the minimum achievable for the HZ entanglement $E_{HZ}^{(1)}$; this minimum is presented for the case $N_1 = 100$ in Fig. 7. Better entanglement is thus achieved by increasing the number of atoms N_1 , provided the other constraints, that $N_2 \gg N_1$ and g_{11} and g_{22} correspond to the critical choice for each mode pair, are satisfied, as shown in Fig. 15. Analytical details are given in the Appendix.

It is interesting that the case of approximately equal couplings $g_{11} = g_{22} = g_{12}$ is generally less favorable for the HZ spin entanglement (Figure 14). This can be understood if we rewrite the Hamiltonian (V.10) in terms of

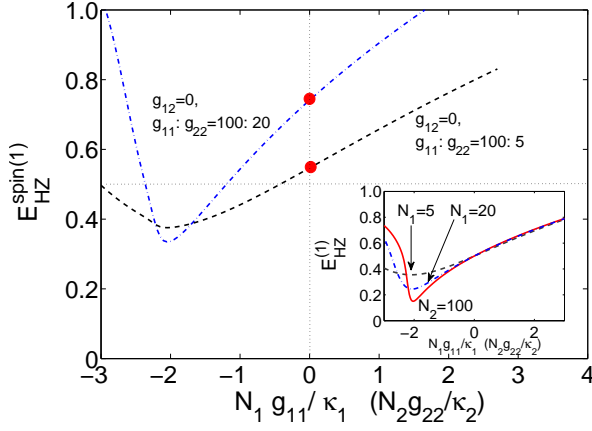


Figure 15. Entanglement using adiabatic cooling to ground state in a two-well potential, at $T = 0K$. Here $\kappa = \kappa_1 = \kappa_2$, $g_{12} = 0$, and both g_{11} and g_{22} are varied so that $N_1 g_{11}/\kappa_1 = N_2 g_{22}/\kappa_2$. $E_{HZ}^{spin(1)} < 1$ indicates entanglement; $E_{HZ}^{spin(1)} < 0.5$ indicates EPR steering. Main graph: (black dashed curve) $N_1 = 5$, $N_2 = 100$; (blue dotted curve) $N_1 = 20$, $N_2 = 100$. The curves are for values of local coupling that optimize $E_{HZ}^{(1)}$ for each mode pair, in which case for $N_2 \gg N_1$ the $E_{HZ}^{spin(1)}$ becomes the $E_{HZ}^{(1)}$ displayed in Fig. 7. The inset reveals the individual degree of HZ entanglement $E_{HZ}^{(1)}$ for the mode pairs a_1, b_1 and a_2, b_2 , as explained in the text.

the spin operators. We obtain $H \simeq \chi (J_A^Z)^2 + \chi (J_B^Z)^2 + \kappa(a_1^\dagger b_1 + a_1 b_1^\dagger + a_2^\dagger b_2 + a_2 b_2^\dagger)$, where $\chi \simeq \frac{1}{2}(g_{11} + g_{22} - 2g_{12})$ gives the effective nonlinearity, and those terms related to $J_{A,B}^Z$, $N_{1,2}^2$, $N_{1,2}$ have been omitted. For equal couplings $g_{12} = g_{11} = g_{22}$, the Hamiltonian thus effectively reduces to the linear term of the BS model of Fig. 12. This is evident in the results of Figs. 14 and 15. Furthermore, enhancement of the nonlinearity is possible, if g_{12} becomes negative. The green solid curve of Figure 14 shows an enhanced entanglement for negative local cross-coupling, $g_{12} < 0$.

The spin HZ entanglement is optimal in the attractive regime, $g_{11} < 0$. Enhancement of entanglement in the repulsive regime is possible (Figure 16), if one examines the spin HZ entanglement for the rotated modes, a' , b' of Eq. (IV.10).

The effect of temperature is given in Fig. 17. In our calculations, we account for effects of finite temperatures by assuming a canonical ensemble of $\rho = \exp[-H/k_B T]$, with an inter-well coupling of $\kappa/k_B = 50nK$. The critical temperature for EPR entanglement signature is shown in Fig. 17.

The predictions in this paper are based on the assumption that the total number N of atoms is fixed. Entanglement ($E_{HZ}^{(1)} = 0.5$), though not EPR-steering, is obtainable between the output ports of a beam splitter with a number (Fock) state input, in the absence of nonlinear coupling terms, as was shown in Sections IV.B and V.B. However, for coherent state inputs, which have a Poissonian number distribution, this entanglement is not

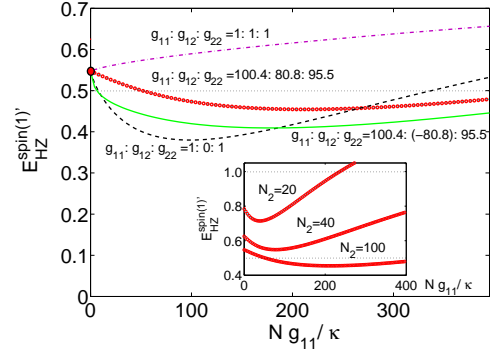


Figure 16. (Color online) Adiabatic cooling to ground state in a two-well potential, at $T = 0K$. Here $\kappa = \kappa_1 = \kappa_2$. Parameters are as for Fig. 14, but the entanglement parameter is calculated for the rotated modes a' , b' of Eq. (IV.10). For large N_2 , the strength of entanglement measure is enough to confirm EPR steering via the criterion Eq. (V.7).

possible [71], and we draw the conclusion that number fluctuations will have an important effect on the entanglement. We have studied this effect in Refs. [29, 61] and suggested in [61] how one can adapt the HZ-entanglement criteria to reduce the sensitivity to atom number fluctuations. The effect of particle fluctuations on entanglement and precision measurement has been studied recently by Hyllus et al [72]. However, such modifications have not been studied in this case for the EPR steering type of nonlocality.

3. Asymmetric tunneling case

An alternative strategy more closely aligned to those used in optics is to consider $\kappa_2 = 0$, $\kappa_1 \neq 0$. In this case, the modes a_2 and b_2 are uncoupled and independent. If they are prepared in coherent states $|\alpha_2\rangle|\beta_2\rangle$ (we take $\alpha_2 = \beta_2 = \alpha$, where α is real), with α large, the entanglement $E_{HZ}^{spin(1)}$ approaches the value given in the two-mode case, by $E_{HZ}^{(1)}$. We explain this as follows. For independent modes, as shown by equation (VI.7) of the Appendix, the HZ spin entanglement criterion (V.2) becomes, upon assuming coherent states for a_2 and b_2 ,

$$|\langle a_1^\dagger b_1 \rangle|^2 \alpha^4 > \langle a_1^\dagger a_1 b_1^\dagger b_1 \rangle (1 + \alpha^2)^2 \quad (\text{V.11})$$

which we see will approach the required two-mode entanglement level in the limit of large α . Figure 18 plots the result with finite numbers of atoms for the case of optimal $E_{HZ}^{(1)}$ which occurs at $N_1 g_{11}/\kappa_1 \approx -2.03$ when $N_1 = 100$. We can see that the four mode EPR entanglement achieved ($C_J/J \approx 0.15$) is that of the two-mode case (Fig. 7) provided there is a large enough number of atoms in the second mode.

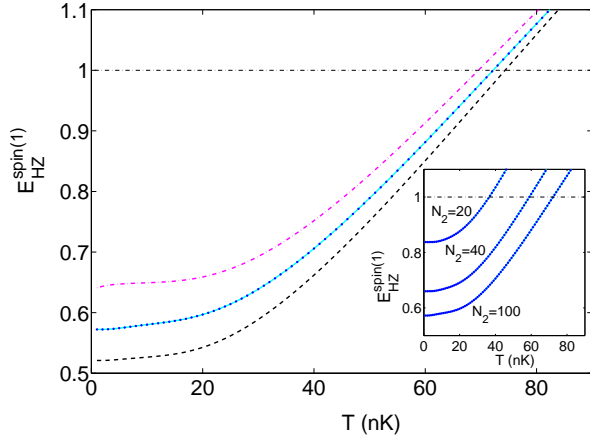


Figure 17. (Color online) The effect of critical temperatures corresponding to the parameters of Fig. 14 when $Ng/\kappa \approx -2.23$.

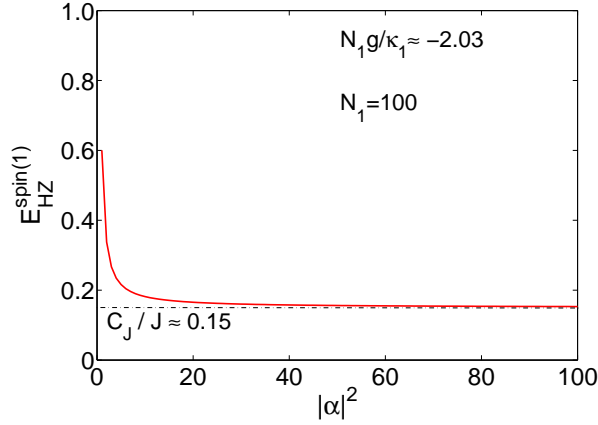


Figure 18. (Color online) The effect of an uncorrelated coherent atomic oscillator field for mode 2 in a coherent state with amplitude α , in the optimal case of Fig. 7 when $N_1 g/\kappa \approx -2.03$.

VI. SUMMARY

We have examined a number of strategies capable of generating detectable entanglement between two spatially-separated potential wells in a BEC. These include both two and four-mode strategies similar to those already used for spin-squeezing, but generalized to a double well. The model used to calculate the relevant variances has been shown to give a good fit to experimental data [25, 64]. Our results find that local cross couplings can have a strong effect on entanglement, and results for the EPR entanglement improve with higher atom numbers. We find that a spin version of the Hillery-Zubairy (HZ) entanglement criterion appears readily suited to analyzing entanglement and the EPR paradox in these experiments. Furthermore, we have shown that the HZ entanglement criteria give information about the number of particles involved in the entangled state and, through

higher order moments, the nature of the multiparticle entanglement.

ACKNOWLEDGMENTS

This research was supported by an Australian Research Council Discovery grant. We wish to acknowledge useful discussions with M. K. Oberthaler, C. Gross, P. Treutlein, A. I. Sidorov, M. Egorov and B. Opanchuk.

APPENDIX A

The system generally is described by a density matrix $\rho = \sum_R P_R \rho^R$. Each ρ^R is a pure state with a mean total number N^R of atoms in modes a and b . The sums of the variances must be greater than the average of the variances of each component of the mixture [73]. The spin operators are defined according to (IV.1). We now suppose the maximum number of atoms in any component to be n_0 . Then the maximum spin for any such component is $J_0 = n_0/2$. Then we are able to conclude that $\{(\Delta_R J_{AB}^X)^2 + (\Delta_R J_{AB}^Y)^2\}/(N^R/2) \geq C_{J_0}/J_0$ because the functions C_{J_0}/J_0 decrease monotonically with increasing J_0 , as shown in the Ref. [59]. This leads to:

$$\begin{aligned} (\Delta J_{AB}^X)^2 + (\Delta J_{AB}^Y)^2 &\geq \sum_R P_R \{(\Delta_R J_{AB}^X)^2 + (\Delta_R J_{AB}^Y)^2\} \\ &\geq \sum_R P_R (N^R/2) C_{J_0}/J_0 \end{aligned} \quad (\text{VI.1})$$

Factorizing and using $\langle N \rangle = \sum_R P_R N^R$ gives the final result

$$E_{HZ} = \frac{(\Delta J_{AB}^X)^2 + (\Delta J_{AB}^Y)^2}{\langle \hat{N}_{AB} \rangle / 2} \geq C_{n_0/2}/(n_0/2). \quad (\text{VI.2})$$

The observation of $E_{HZ} < C_{n_0/2}/(n_0/2)$ thus implies that the two mode entangled state consists of *more* than n_0 atoms in total, that is, that there are necessarily more than n_0 atoms entangled. In this case, the spin $J_{AB}^{X/Y}$ measurement must be compatible with $J_{AB}^{X/Y}$ as defined in terms of just two modes, a and b .

APPENDIX B

The system generally is described by a density matrix $\rho = \sum_R P_R \rho_{sep}^R + \sum_{R'} P_{R'} \rho_{ent}^{R'}$, where ρ_{sep}^R and $\rho_{ent}^{R'}$ represent pure separable and entangled states respectively. The higher-order HZ entanglement measure can therefore be written as a ratio

$$R = \frac{|\langle a^m (b^\dagger)^m \rangle|^2}{\langle (a^\dagger)^m a^m (b^\dagger)^m b^m \rangle} \quad (\text{VI.3})$$

where

$$\langle a^m (b^\dagger)^m \rangle = \sum_R P_R \langle a^m (b^\dagger)^m \rangle_R + \sum_{R'} P_{R'} \langle a^m (b^\dagger)^m \rangle_{R'}$$

and

$$\begin{aligned} \langle (a^\dagger)^m a^m (b^\dagger)^m b^m \rangle &= \sum_R P_R \langle (a^\dagger)^m a^m (b^\dagger)^m b^m \rangle_R \\ &+ \sum_{R'} P_{R'} \langle (a^\dagger)^m a^m (b^\dagger)^m b^m \rangle_{R'} \end{aligned}$$

Here $\langle O \rangle_R$ represents the expectation value of O for state ρ_R . Since for a separable state, $R \leq 1$, we can see that if $\sum_{R'} P_{R'} \langle a^m (b^\dagger)^m \rangle_{R'} = 0$, it is always the case that ρ predicts $R < 1$. In short, the higher order entanglement, $E^{(m)} < 1$, cannot be achieved unless there is a nonzero probability $P_{R'}$ for a pure entangled state $\rho_{ent}^{R'}$ for which $\langle a^m (b^\dagger)^m \rangle \neq 0$. Expanding the pure entangled state in terms of the number states yields most generally $\rho = |\psi\rangle\langle\psi|$, where

$$|\psi\rangle = \sum_{n,l} c_{nl} |n\rangle |l\rangle. \quad (\text{VI.4})$$

If only adjacent number states of type $|n\rangle$, $|n+1\rangle$ have nonzero amplitude c_{nl} , the $\langle a^m (b^\dagger)^m \rangle = 0$ where $m > 1$. Hence, the superposition (VI.4) necessarily includes states separated by m .

APPENDIX C

In this Appendix, we show we show how to directly “convert” the inter-well entanglement shown in Fig. 7 to an EPR entanglement, with the use of a “local oscillator”-type treatment which applies where two of the strong local modes are uncorrelated. This is the case of $g_{12} = 0$, illustrated in Fig 2.

Local oscillator measurements are achieved optically by combining a mode with a very strong coherent state [6]. We can achieve something effectively equivalent to a “local oscillator” measurement, where the second pair

of levels a_2 , b_2 are much more heavily populated than levels a_1 and b_1 , by assuming the second pair of modes are in an uncorrelated coherent state. We explain this as follows. Since $J_A^+ = a_1^\dagger a_2$ and $J_A^- = a_1 a_2^\dagger$ and $J_B^+ = b_1^\dagger b_2$ and $J_B^- = b_1 b_2^\dagger$ we can rewrite the criterion (V.2) in terms of the mode operator moments, for this special case, by the factorization that is justified for independent fields at each location. Thus,

$$|\langle J_A^+ J_B^- \rangle|^2 = |\langle a_1^\dagger b_1 \rangle \langle a_2 b_2^\dagger \rangle|^2, \quad (\text{VI.5})$$

and similarly

$$\langle (J_A^+ J_A^-)(J_B^+ J_B^-) \rangle = \langle a_1^\dagger a_2 a_1 a_2^\dagger b_1^\dagger b_2 b_1 b_2^\dagger \rangle. \quad (\text{VI.6})$$

The criterion (V.2) becomes

$$|\langle a_1^\dagger b_1 \rangle|^2 |\langle a_2 b_2^\dagger \rangle|^2 > \langle a_1^\dagger a_1 b_1^\dagger b_1 \rangle \langle (1 + a_2^\dagger a_2)(1 + b_2^\dagger b_2) \rangle \quad (\text{VI.7})$$

Clearly, since the inter-well entanglement studied in Section IV and summarized in Fig. 7 enables $|\langle a_1^\dagger b_1 \rangle|^2 > \langle a_1^\dagger a_1 b_1^\dagger b_1 \rangle$ via the HZ entanglement criterion, we will have (at least) the same level of four mode EPR entanglement, provided

$$|\langle a_2 b_2^\dagger \rangle|^2 \geq \langle (1 + a_2^\dagger a_2)(1 + b_2^\dagger b_2) \rangle. \quad (\text{VI.8})$$

In fact, the inequality would represent violation of the two-site version of the Bell inequality discussed in [57], which is not achievable for this system. However, it is still possible to optimize the EPR entanglement. This can be achieved in the following way. If the two modes a_2 and b_2 are also coupled via an inter-well interaction ($\kappa_2 \neq 0$ in Fig. 2), to produce the ground state solution of Fig 9, then $E_{HZ}^{(1)} < 1$ amounts to $|\langle a_2 b_2^\dagger \rangle|^2 > \langle a_2^\dagger a_2 b_2^\dagger b_2 \rangle$. The optimal $E_{HZ}^{(1)}$ is at $N_2 g_{22} / \kappa_2 \approx -2.03$, while for the modes a_1 and a_2 , the optimal (VI.7) occurs for $N_1 g_{11} / \kappa_1 \approx -2.1$ (inset of Fig. 15). This choice gives enhanced EPR entanglement as shown in Fig. 14. Better entanglement is possible for this optimal choice, as the numbers are increased (Fig. 15).

-
- [1] A. Einstein, B. Podolsky and N. Rosen, Phys. Rev. **47**, 777 (1935).
 - [2] J. S. Bell, Physics **1**, 195 (1965); J. F. Clauser, M. A. Horne, A. Shimony and R. A. Holt, Phys. Rev. Lett. **23**, 880 (1969).
 - [3] J. F. Clauser and A. Shimony, Rep. Prog. Phys. **41**, 1881 (1978).
 - [4] A. Aspect, P. Grangier and Gerard Roger, Phys. Rev. Lett. **49**, 91 (1982); A. Aspect, J. Dalibard and G. Roger, Phys. Rev. Lett. **49**, 1804 (1982).
 - [5] P. G. Kwiat et al., Phys. Rev. Lett. **75**, 4337 (1995); G. Weihs et al., ibid. **81**, 5039 (1998); W. Tittel et al., ibid. **84**, 4737 (2000).
 - [6] Z. Y. Ou et al, Phys. Rev. Lett. **68**, 3663 (1992).
 - [7] M. D. Reid, Phys. Rev. A **40**, 913 (1989).
 - [8] A. K. Ekert, Phys. Rev. Lett. **67**, 661 (1991).
 - [9] D. J. Wineland et al., Phys. Rev. A **50**, 67 (1994).
 - [10] M. J. Holland and K. Burnett, Phys. Rev. Lett. **71**, 1355 (1993).
 - [11] J. P. Dowling, Phys Rev A **57**, 4736 (1998).
 - [12] L. Pezze and A. Smerzi, Phys Rev. Lett. **102**, 100401 (2009).
 - [13] G. Y. Xiang et al., Nature photonics **5**, 43, (2011).
 - [14] T. Opatrny and G. Kurizki, Phys. Rev. Lett. **86**, 3180 (2001); K.V. Kheruntsyan and P. D. Drummond, Phys. Rev. A **66**, 031602(R) (2002); K. V. Kheruntsyan, M. K. Olsen and P. D. Drummond, Phys. Rev. Lett. **95**, 150405 (2005).

- [15] A. A. Norrie, R. J. Ballagh, and C. W. Gardiner, Phys. Rev. Lett. **94**, 040401 (2005); P. Deuar and Peter D. Drummond, Phys. Rev. Lett. **98**, 120402 (2007).
- [16] A. J. Ferris, M. K. Olsen, E. G. Cavalcanti and M. J. Davis, Phys. Rev. A **78**, 060104 (2008); A. J. Ferris, M. K. Olsen and M. J. Davis, Phys. Rev. A **79**, 043634 (2009).
- [17] P. Milman, A. Keller, E. Charron and O. Atabek, Phys. Rev. Lett. **99**, 130405 (2007); Magnus Ögren and K. V. Kheruntsyan, Phys. Rev. A **82**, 013641 (2010).
- [18] C. Orzel, A. K. Tuchman, M. L. Fenselau, M. Yasuda and M. A. Kasevich, Science **291**, 2386 (2001).
- [19] M. Greiner, C. A. Regal, J. T. Stewart and D. S. Jin, Phys. Rev. Lett. **94**, 110401 (2005).
- [20] J.-C. Jaskula, et. al., Phys. Rev. Lett. **105**, 190402 (2010); V. Krachmalnicoff, et. al., Phys. Rev. Lett. **104**, 150402 (2010).
- [21] Robert Bücker, et. al., Nature Physics **7**, 608–611 (2011).
- [22] C. Gross, H. Strobel, E. Nicklas, T. Zibold, N. Bar-Gill, G. Kurizki and M. K. Oberthaler, Nature **480**, 219 (2011).
- [23] B. Lücke, et. al., Science **334**, 773 (2011).
- [24] J. Esteve, et. al., Nature **455**, 1216 (2008).
- [25] C. Gross, T. Zibold, E. Nicklas, J. Esteve and M. K. Oberthaler, Nature (London) **464**, 1165 (2010).
- [26] M. F. Riedel, P. Böhi, Y. Li, T.W. Hänsch, A. Sinatra and P. Treutlein, Nature (London) **464**, 1170 (2010).
- [27] M. Egorov, et. al., Phys. Rev. A **84**, 021605 (2011).
- [28] N. Bar-Gill, et. al., Phys. Rev. Lett. **106**, 120404 (2011).
- [29] Q. Y. He, et. al., Phys. Rev. Lett. **106**, 120405 (2011).
- [30] M. D. Reid, et. al., Rev. Mod. Phys. **81**, 1727 (2009).
- [31] E. Schroedinger, Naturwiss. **23**, 807 (1935); Proc. Cambridge Philos. Soc. **31**, 555 (1935); Proc. Cambridge Philos. Soc. **32**, 446 (1936).
- [32] H. M. Wiseman, S. J. Jones and A. C. Doherty, Phys. Rev. Lett. **98**, 140402 (2007).
- [33] S. J. Jones, H. M. Wiseman and A. C. Doherty, Phys. Rev. A **76**, 052116 (2007).
- [34] D. J. Saunders, et al, Nature Physics **6**, 845 (2010).
- [35] E. G. Cavalcanti, et al, Phys. Rev. A **80**, 032112 (2009).
- [36] E. G. Cavalcanti, et al, Phys. Rev. A **84**, 032115 (2011).
- [37] L. M. Duan, G. Giedke, J. I. Cirac and P. Zoller, Phys. Rev. Lett. **84**, 2722 (2000).
- [38] R. Simon, Phys. Rev. Lett. **84**, 2726 (2000).
- [39] V. Giovannetti, S. Mancini, D. Vitali and P. Tombesi, Phys. Rev. A **67**, 022320 (2003).
- [40] A. Peng and A. S. Parkins, Phys. Rev. A **65**, 062323 (2002); Q. Y. He et al., Phys. Rev. A **79**, 022310 (2009); Q. Y. He, et al, Optics Express **17**, 9662 (2009).
- [41] B. L. Schumaker and Carlton M. Caves, Phys. Rev. A **31**, 3093 (1985).
- [42] M. D. Reid and P. D. Drummond, Phys. Rev. Lett. **60**, 2731 (1988).
- [43] A. Heidmann et al, Phys. Rev. Lett. **59**, 2555 (1987).
- [44] A. S. Lane et al, Phys Rev Lett. **60**, 1940 (1988); Phys. Rev. A, **38**, 788 (1988).
- [45] R. E. Slusher, et al., Phys. Rev. Lett. **55**, 2409 (1985). M. D. Reid and D. F. Walls, Phys. Rev. A **33**, 4465 (1986).
- [46] P. Kinsler et al, Phys. Rev. A **48**, 3310-3320 (1993).
- [47] K. Dechoum, et al, Phys. Rev. A **70**, 053807 (2004).
- [48] J. I. Cirac, M. Lewenstein, K. Molmer and P. Zoller, Phys. Rev. A **57**, 1208 (1998); G. Mazzarella, L. Salasnich, A. Parola and F. Toigo, Phys. Rev. A **83**, 053607 (2011); C. Bodet, J. Estève, M. K. Oberthaler and T. Gasenzer, Phys. Rev. A **81**, 063605 (2010).
- [49] G. J. Milburn, J. Corney, E. M. Wright and D. F. Walls, Phys. Rev. A **55**, 4318 (1997).
- [50] T. J. Haigh, A. J. Ferris, and M. K. Olsen, Opt. Commun. **283**, 3540 (2010).
- [51] J. Dunningham and K. Burnett, Journ. Modern Optics **48**, 1837, (2001).
- [52] D. Gordon and C. M. Savage, Phys Rev A **59**, 4623 (1999).
- [53] L. D. Carr, D. R. Dounas-Frazer and M. A. Garcia-March, Europhysics Lett. **90**, 10005 (2010).
- [54] P. D. Drummond, R. M. Shelby, S. R. Friberg and Y. Yamamoto, Nature **365**, 307-313 (1993); Oliver Glöckl et al J. Opt. B: Quantum Semiclass. Opt. **5**, S492 (2003).
- [55] W. P. Bowen, N. Treps, R. Schnabel, and P. K. Lam, Phys. Rev. Lett. **89**, 253601 (2002).
- [56] M. Hillery and M. S. Zubairy, Phys. Rev. Lett. **96**, 050503 (2006).
- [57] E. G. Cavalcanti, C. J. Foster, M. D. Reid, and P. D. Drummond, Phys. Rev. Lett. **99**, 210405 (2007).
- [58] Q. Sun, H. Nha, and M. S. Zubairy, Phys. Rev. A **80**, 020101(R) (2009).
- [59] Q. Y. He, Shi-Guo Peng, P. D. Drummond, and M. D. Reid, Phys. Rev. A **84**, 022107 (2011).
- [60] A. S. Sørensen and K. Molmer, Phys. Rev. Lett. **86**, 4431 (2001).
- [61] Q. Y. He, T. Vaughan, P. D. Drummond and M. D. Reid, to be published.
- [62] Andrew P. Hines, Ross H. McKenzie, and Gerard J. Milburn, Phys. Rev. A **67**, 013609 (2003).
- [63] Q. Xie and W. Hai, Eur. Phys. J. D **39**, 277 (2006).
- [64] M. D. Reid, Q. Y. He, and P. D. Drummond, to be published, Frontiers of Physics.
- [65] M. Hillery, H. T. Dung, and J. Niset, Phys. Rev. A **80**, 052335 (2009).
- [66] H. Zheng, H. T. Dung, and M. Hillery, Phys. Rev. A **81**, 062311 (2010).
- [67] M. Hillery, H. T. Dung, and H. Zheng, Phys. Rev. A **81**, 062322 (2010).
- [68] E. G. Cavalcanti and M. D. Reid, Journ. Mod. Opt. **54**, 2373 (2007).
- [69] E. G. Cavalcanti, et al, Optics Express **17**, 18693 (2009).
- [70] Q. Y. He, P. D. Drummond, and M. D. Reid, Phys. Rev. A **83**, 032120 (2011).
- [71] B. E. Salah, D. Stoler, and M. C. Teich, Phys Rev A **27**, 360 (1983).
- [72] P. Hyllus, L. Pezze and A. Smerzi, arXiv: 1003.0649 (2010).
- [73] H. F. Hofmann and S. Takeuchi, Phys. Rev. A **68**, 032103 (2003).